

Optimising Gaussian processes for reconstructing dark energy dynamics from supernovae

Marina Seikel^{1,2} and Chris Clarkson²

¹*Department of Physics, University of the Western Cape, Cape Town 7535, South Africa*

²*Astrophysics, Cosmology & Gravity Centre, and,
Department of Mathematics & Applied Mathematics,
University of Cape Town, Cape Town 7701, South Africa*

Gaussian processes are a fully Bayesian smoothing technique that allows for the reconstruction of a function and its derivatives directly from observational data, without assuming a specific model or choosing a parameterization. This is ideal for constraining dark energy because physical models are generally phenomenological and poorly motivated. Model-independent constraints on dark energy are an especially important alternative to parameterized models, as the priors involved have an entirely different source so can be used to check constraints formulated from models or parameterizations. A critical prior for Gaussian process reconstruction lies in the choice of covariance function. We show how the choice of covariance function affects the result of the reconstruction, and present a choice which leads to reliable results for present day supernovae data. We also introduce a method to quantify deviations of a model from the Gaussian process reconstructions.

I. INTRODUCTION

The Λ CDM of cosmology has been very successful in describing observations of various data. While it is the simplest model that is consistent with the data, there is a plethora of other viable cosmological models (for reviews see [1, 2]). A common approach is to fit these models to the data and apply model selection techniques to determine the most likely theory.

An alternative approach is to perform model-independent reconstructions, which can be used to determine deviations from Λ CDM. This is particularly important when physical models are poorly motivated from a fundamental theory, as is the case for most dark energy models. A range of consistency tests have been introduced to probe various aspects of Λ CDM [3–8]. For these tests it is crucial to use a non-parametric method to reconstruct functions such as the luminosity distance $d_L(z)$ or the Hubble rate $H(z)$. Gaussian processes (GP) provide such a method, which is also capable of reliably reconstructing derivatives of a function. GP have been applied to this problem in cosmology in [8–16].

In this work, we focus on some aspects of GP reconstructions of dark energy from supernova (SN) data. The luminosity distance is given by

$$d_L(z) = \frac{c(1+z)}{H_0\sqrt{-\Omega_k}} \sin\left(\sqrt{-\Omega_k} \int_0^z dz' \frac{H_0}{H(z')}\right), \quad (1)$$

where

$$H(z)^2 = H_0^2 \left\{ \Omega_m(1+z)^3 + \Omega_k(1+z)^2 + (1 - \Omega_m - \Omega_k) \exp\left[3 \int_0^z \frac{1+w(z')}{1+z'} dz'\right] \right\}. \quad (2)$$

Using the dimensionless comoving distance

$$D(z) = (H_0/c)(1+z)^{-1}d_L(z), \quad (3)$$

we can write the equation of state $w(z)$ as

$$w(z) = \{2(1+z)(1+\Omega_k D^2)D'' - [(1+z)^2\Omega_k D'^2 + 2(1+z)\Omega_k D D' - 3(1+\Omega_k D^2)]D'\} / \{3\{(1+z)^2[\Omega_k + (1+z)\Omega_m]D'^2 - (1+\Omega_k D^2)\}D'\}, \quad (4)$$

where $' = d/dz$.

Reconstructing $w(z)$ from distance data requires the knowledge of the density parameters Ω_m and Ω_k . As there are degeneracies between the density parameters and the equation of state [9, 17–19], these quantities cannot be determined by considering distance measurements only. In this work, we only use mock data sets and thus have the luxury of being able to fix the values for the density parameters. We use $\Omega_m = 0.3$ and $\Omega_k = 0$ throughout the paper. In practice, these degeneracies are problematic. Despite these concerns, we focus on the reconstruction of $w(z)$ with fixed density parameters in this work because our main interest here is to analyze how well the input model (which is determined by its equation of state) can be recovered by GP reconstructions. While we focus on the reconstruction of w , we also reconstruct the deceleration parameter,

$$q(z) = -(1+z)D''(z)/D'(z) - 1, \quad (5)$$

for some tests.

For a non-parametric regression method such as GP, our aim is to produce confidence limits such that we trap the true function appropriately. For example, for repeated realisations of a data set for a given model we require that our confidence limit of 95% traps the correct model in 95% of realisations. For w we are not just trying to reconstruct a function from data, but a complicated function of its first and second derivatives as well. This makes it a much more complicated problem for which we need to identify appropriate covariance functions which can reproduce expected models accurately. We introduce a family of 4 $w(z)$'s in addition to Λ CDM of increasing complexity which we attempt to reconstruct with a fixed

number of SNIa (about 500). These models are not intended to be physical, but rather to illustrate the types of features we might be able to constrain. We analyse 4 different covariance functions which each have one amplitude parameter and one length parameter. These are a simple Gaussian, and 3 functions of the Matérn class. The main difference between these is the widths of their peaks which influence the strength of the correlations between function points at different redshifts. We identify the one which gives the most accurate confidence limits for the number of SNIa we consider. Clearly, for 500 SNIa we can only expect to reconstruct one ‘feature’ in w , but it is still important that for more complicated w we trap the function appropriately.

This work is structured as follows: The basics of GP reconstruction are summarized in section II. Section III lists the models for which we create mock data sets. Section IV provides several example reconstructions. In section V, we perform coverage tests which determine the reliability of the error bars of the reconstructions. These tests allow us to choose a suitable covariance function. We introduce a method to determine deviations of a model from the GP reconstructions in section VI and conclude in section VII.

II. GAUSSIAN PROCESSES

GP provide a technique to reconstruct a function from observational data without assuming a specific parameterization. Derivatives of the function can also be reliably reconstructed. A detailed description of GP can be found in the book by Rasmussen and Williams [20], which we will follow throughout this work. We use GaPP¹ (Gaussian Processes in Python), which is a freely available GP package developed by Seikel. It was introduced in [9] and has recently been expanded to allow for marginalization over hyperparameters using the MCMC package emcee² [21].

A. Gaussian process reconstructions

Assume we have N observational data points $\mathbf{y} = (y_1, \dots, y_N)$ at redshifts $\mathbf{Z} = (z_1, \dots, z_N)$. The errors of the observations are given in the covariance matrix C . We want to reconstruct the function underlying the data at points $\mathbf{Z}^* = (z_1^*, \dots, z_N^*)$ and denote the function values at these points as $\mathbf{f}^* = (f(z_1^*), \dots, f(z_N^*))$.

GP can be thought of as a generalization of a Gaussian distribution: At each point z^* , the reconstructed function $f(z^*)$ is described by normal distribution. Function values at different points z^* and \tilde{z}^* are not independent

from each other, but are related by a covariance function $k(z^*, \tilde{z}^*)$ (see section II C for some choices of k). Covariance functions depend on hyperparameters, such as the signal variance σ_f and the characteristic length scale ℓ . (More complicated covariance functions can depend on additional hyperparameters; but in this work, we will focus on covariance functions that only include σ_f and ℓ .) In contrast to regular parameters, hyperparameters do not specify the form of a function; they only characterize typical changes of the reconstructed function. ℓ roughly corresponds to the scale in z over which significant changes occur in the function values and σ_f denotes the typical size of these changes.

For a given covariance function and hyperparameters, the reconstructed function is determined by the covariances between the data and the points \mathbf{Z}^* , where the function is to be reconstructed. The relevant covariances are given by matrices $K(\mathbf{X}, \tilde{\mathbf{X}})$ with $\{K(\mathbf{X}, \tilde{\mathbf{X}})\}_{ij} = k(x_i, \tilde{x}_j)$, where $\mathbf{X}, \tilde{\mathbf{X}} \in \{\mathbf{Z}, \mathbf{Z}^*\}$.

The mean and covariance of the GP reconstruction of the n th derivative of a function are given by

$$\overline{\mathbf{f}^{*(n)}} = K^{(n,0)}(\mathbf{Z}^*, \mathbf{Z}) [K(\mathbf{Z}, \mathbf{Z}) + C]^{-1} \mathbf{y} \quad (6)$$

and

$$\text{cov}(\mathbf{f}^{*(n)}) = K^{(n,n)}(\mathbf{Z}^*, \mathbf{Z}^*) - K^{(n,0)}(\mathbf{Z}^*, \mathbf{Z}) [K(\mathbf{Z}, \mathbf{Z}) + C]^{-1} K^{(0,n)}(\mathbf{Z}, \mathbf{Z}^*) \quad (7)$$

respectively. Here, $k^{(n,m)}$ denotes the n th derivative of k with respect to the first argument and the m th derivative with respect to the second argument.

Besides the data, the above equations also depend on the covariance function and the values of the hyperparameters. While the covariance function needs to be chosen by hand, one can either determine the optimal hyperparameters by maximizing the marginal likelihood $\mathcal{L} = p(\mathbf{y}|\mathbf{Z}, \sigma_f, \ell)$, or one can marginalize over this likelihood. (The term ‘marginal likelihood’ refers to the fact that one marginalizes over all possible functions $f(z)$.) In both cases, the hyperparameters are determined by the data. The log marginal likelihood is given by:

$$\begin{aligned} \ln \mathcal{L} &= \ln p(\mathbf{y}|\mathbf{Z}, \sigma_f, \ell) \\ &= -\frac{1}{2} \mathbf{y}^T [K(\mathbf{Z}, \mathbf{Z}) + C]^{-1} \mathbf{y} \\ &\quad - \frac{1}{2} \ln |K(\mathbf{Z}, \mathbf{Z}) + C| - \frac{n}{2} \ln 2\pi. \end{aligned} \quad (8)$$

Recall that K depends on the hyperparameters σ_f and ℓ .

From a Bayesian point of view, marginalizing over the hyperparameters is the correct approach. This is, however, computationally much more expensive than optimizing the hyperparameters. In most cases, the optimization approach is a good approximation. Problems with this approximation can occur if the likelihood \mathcal{L} has multiple (equally high) peaks. However, we have not encountered these problems when reconstructing dark energy. We show below that the difference between the two is close, and so justify using the optimization approach.

¹ <http://www.acgc.uct.ac.za/~seikel/GAPP/index.html>

² <http://github.com/dfm/emcee>

B. Reconstructing $g(f(z), f'(z), \dots)$

Often we are not only interested in a function $f(z)$ for which we have observational data, but also in functions $g(f(z), f'(z), \dots)$ which depend on $f(z)$ and its derivatives. It is important to note that $f(z)$ and its derivatives are not independent quantities. Therefore, we need to consider the covariances

$$\begin{aligned} \text{cov}(\mathbf{f}^{*(n)}, \mathbf{f}^{*(m)}) &= K^{(n,m)}(\mathbf{Z}^*, \mathbf{Z}^*) \\ &- K^{(n,0)}(\mathbf{Z}^*, \mathbf{Z}) [K(\mathbf{Z}, \mathbf{Z}) + C]^{-1} K^{(0,m)}(\mathbf{Z}, \mathbf{Z}^*) \end{aligned} \quad (9)$$

when reconstructing $g(f(z), f'(z), \dots)$.

At each point z^* , we perform a Monte Carlo sampling to obtain the distribution of function values for $g^* = g(f^*, f^{*'}, \dots)$, where $f^* = f(z^*)$. In each sampling step, we draw values for $f^*, f^{*'}, \dots$ from a multivariate normal distribution:

$$\begin{bmatrix} f^* \\ f^{*'} \\ \vdots \end{bmatrix} \sim \mathcal{N} \left(\begin{bmatrix} \overline{f^*} \\ \overline{f^{*'}} \\ \vdots \end{bmatrix}, \begin{bmatrix} \text{cov}(f^*, f^*) & \text{cov}(f^*, f^{*'}) & \dots \\ \text{cov}(f^*, f^{*'}) & \text{cov}(f^{*'}, f^{*'}) & \dots \\ \vdots & \vdots & \ddots \end{bmatrix} \right). \quad (10)$$

These values are used to calculate g^* . Performing many of these MCMC steps, we obtain a distribution of function values for g at each redshift z^* .

C. Covariance functions

There is a large variety of covariance functions. The optimal choice of covariance function depends on the problem at hand (see [20] for some examples). Here, we consider the squared exponential, which is considered to be a general purpose covariance function, and the Matérn class, from which individual covariance functions can be obtained by choosing the parameter ν , which governs the width of the peak of the covariance function for a given ℓ .

The squared exponential and the Matérn class are given by:

Squared exponential:

$$k(z, \tilde{z}) = \sigma_f^2 \exp\left(-\frac{(z - \tilde{z})^2}{2\ell^2}\right) \quad (11)$$

Matérn:

$$\begin{aligned} k(z, \tilde{z}) &= \sigma_f^2 \frac{2^{1-\nu}}{\Gamma(\nu)} \left(\frac{\sqrt{2\nu(z - \tilde{z})^2}}{\ell} \right)^\nu \\ &\times K_\nu \left(\frac{\sqrt{2\nu(z - \tilde{z})^2}}{\ell} \right), \end{aligned} \quad (12)$$

where K_ν is a modified Bessel function. ν is a positive parameter which defines the shape of the covariance

function. While $\nu = 1/2$ corresponds to an exponential $k(z, \tilde{z}) = \sigma_f^2 \exp(-|z - \tilde{z}|/\ell)$, we recover the squared exponential covariance function for $\nu \rightarrow \infty$. The Matérn covariance function is n -times mean square differentiable (i.e. the derivative $\partial^{2n}k(z, \tilde{z})/\partial z^n \partial \tilde{z}^n$ exists and is finite) if and only if $\nu > n$. A covariance function that is n -times mean square differentiable can be used to reconstruct up to the n th derivative of a function.

For half-integer values of ν , the Matérn covariance function can be simplified. Here we consider $\nu = 5/2$, $\nu = 7/2$ and $\nu = 9/2$. The reconstruction of the equation of state from distance data requires the reconstruction of the second derivative $D''(z)$ (see Eq. (4)). Therefore, the smoothness parameter ν needs to be larger than 2. In the following, the Matérn functions with $\nu = 5/2$, $\nu = 7/2$ and $\nu = 9/2$ will be referred to as Matérn(5/2), Matérn(7/2) and Matérn(9/2), respectively. These functions are given by:

Matérn(5/2):

$$\begin{aligned} k(z, \tilde{z}) &= \sigma_f^2 \exp\left[-\frac{\sqrt{5}|z - \tilde{z}|}{\ell}\right] \\ &\times \left(1 + \frac{\sqrt{5}|z - \tilde{z}|}{\ell} + \frac{5(z - \tilde{z})^2}{3\ell^2}\right) \end{aligned} \quad (13)$$

Matérn(7/2):

$$\begin{aligned} k(z, \tilde{z}) &= \sigma_f^2 \exp\left[-\frac{\sqrt{7}|z - \tilde{z}|}{\ell}\right] \\ &\times \left(1 + \frac{\sqrt{7}|z - \tilde{z}|}{\ell} + \frac{14(z - \tilde{z})^2}{5\ell^2} + \frac{7\sqrt{7}|z - \tilde{z}|^3}{15\ell^3}\right) \end{aligned} \quad (14)$$

Matérn(9/2):

$$\begin{aligned} k(z, \tilde{z}) &= \sigma_f^2 \exp\left[-\frac{3|z - \tilde{z}|}{\ell}\right] \\ &\times \left(1 + \frac{3|z - \tilde{z}|}{\ell} + \frac{27(z - \tilde{z})^2}{7\ell^2} \right. \\ &\quad \left. + \frac{18|z - \tilde{z}|^3}{7\ell^3} + \frac{27(z - \tilde{z})^4}{35\ell^4}\right) \end{aligned} \quad (15)$$

Figure 1 shows all four covariance functions considered in this work. Increasing the parameter ν of the Matérn class widens the peak of the function. We get the widest peak for the squared exponential, which corresponds to Matérn($\nu \rightarrow \infty$).

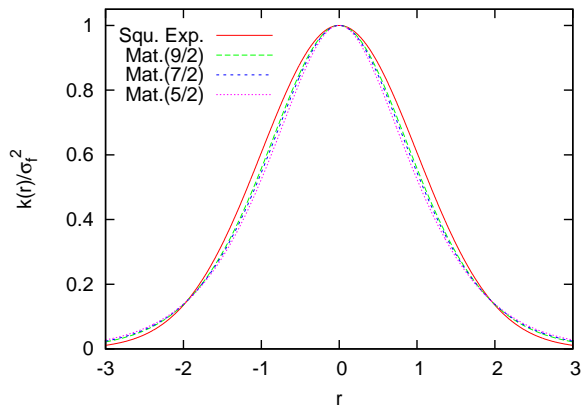


FIG. 1. Different covariance functions $k(r)/\sigma_f^2$ as a function of $r = (z - \tilde{z})/\ell$. Shown are the squared exponential and three functions of the Matérn class with $\nu = 9/2, 7/2, 5/2$.

III. MOCK DATA

We create mock SN data catalogues for different cosmological models. Each model represents a specific smoothness of the equation of state, and is not supposed to represent a specific model. $w(z)$ for the five test models is listed in table I and shown in figure 2. Also shown are the dimensionless comoving distance $D(z)$ and the residual distance $D(z) - D_{\Lambda\text{CDM}}(z)$. For easier reference, we have assigned the names “smooth”, “peak”, “bumpy” and “noisy” to the non- ΛCDM models. We assume all models to be spatially flat ($\Omega_k = 0$) and fix the matter density to $\Omega_m = 0.3$.

We use the scatter anticipated for the Dark Energy Survey (DES) [22] to create the mock data. However, instead of using the anticipated number of ~ 4000 SNe, we reduced this number to 546 to speed up the analysis. For real life observations the errors are Gaussian in magnitude. Here, we also assume the errors to be Gaussian in distance D as GP require the observational errors to be Gaussian. This assumption is justified because the actual errors in D deviate only slightly from Gaussianity for the considered scatter.

IV. EXAMPLE RECONSTRUCTIONS

In this section, we show some example reconstructions. This gives some intuition of how different methods can affect the result of a reconstruction. However, isolated examples are not suitable to determine which approach leads to the most reliable results for a given problem. In order to determine that one needs to analyze many reconstructions instead of just a few examples. This is done in sections V and VI.

ΛCDM	$w(z) = -1$
smooth	$w(z) = \frac{1}{2}(-1 + \tanh[3(z - \frac{1}{2})])$
peak	$w(z) = -1 + 0.7 \exp\left[-\left(\frac{z-0.5}{0.2}\right)^2\right]$
bumpy	$w(z) = -0.9 - 0.1 \cos(3.5z) + 0.1 \sin(10z)$
noisy	$w(z) = -0.9 + 0.05 \sin(2.5z) - 0.055 \cos(5.7z)$ $- 0.06 \sin(8.9z) + 0.03 \cos(14.2z)$ $- 0.07 \cos(19.4z) + 0.06 \sin(27.1z)$ $+ 0.034 \cos(33.8z) - 0.047 \sin(47.2z)$ $- 0.027 \cos(77.8z) + 0.032 \sin(117.8z)$

TABLE I. $w(z)$ for the different test models. From top to bottom the models become increasingly complex, and serve as suitable benchmark models to quantify the sorts of behaviour that can be constrained for a given number of SNIa.

A. Marginalization vs. optimization

As mentioned in section II A, marginalization over the hyperparameters would be the correct Bayesian approach. As this method is computationally much more expensive than optimizing the hyperparameters by maximizing the marginal likelihood (8), it can become prohibitive for large data sets. Optimization is much faster and in most cases provides good results. While we focus on the optimization method in this work, we show some example reconstructions to compare the two different approaches in this section.

Figure 3 shows reconstructions of the equation of state $w(z)$ for two realisations of mock ΛCDM data sets. Here, we have used the squared exponential covariance function. The reconstructions have once been performed by optimizing the hyperparameters and once by marginalizing over them. In all cases, the value of the input model, $w = -1$, is captured within the 95% confidence limits (CL) of the reconstruction. Note that marginalization does not necessarily lead to increased errors, which can be clearly seen for realisation B.

For a given realisation, it is not obvious which approach leads to a reconstruction that resembles the input model more closely than the other approach. For realisation A, the reconstructed mean is very close to the theoretical value up to $z \sim 1$ when marginalizing over the hyperparameter. Using the optimisation approach, the mean seems less stable. But for realisation B, the mean and 68% CL indicate an increase in w for the marginalisation approach (the 95% CL still captures $w = -1$), while optimization resembles ΛCDM more closely.

However note that we do expect the input model to leave the 68% CL limits for a part of the redshift range for at least some of the realisations. Therefore, a closer resemblance of the input model does not necessarily indicate a better method. See sections V and VI for a detailed analysis.

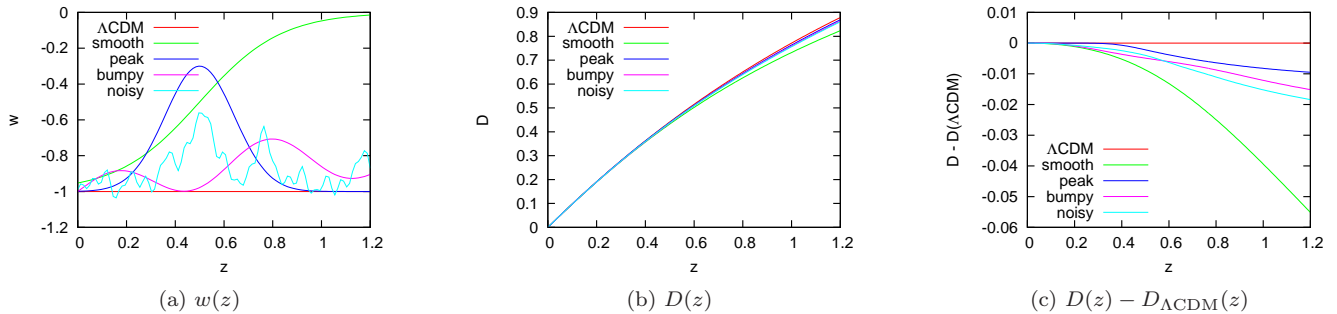


FIG. 2. $w(z)$, $D(z)$ and $D(z) - D_{\Lambda\text{CDM}}(z)$ for the different test models.

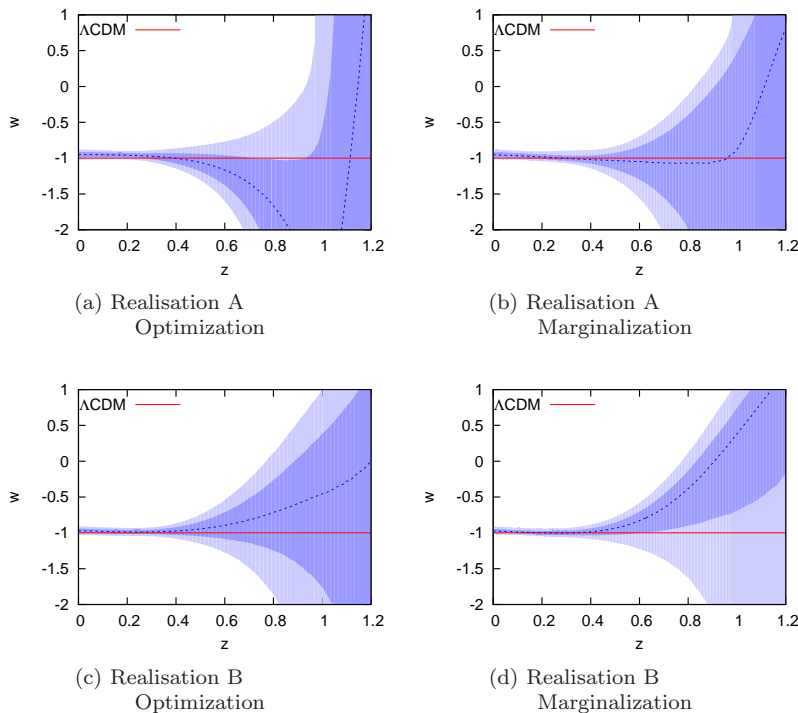


FIG. 3. Gaussian process reconstructions of $w(z)$ for two realisations of a mock data set. The blue (dotted) line is the mean of the reconstruction and the blue shaded regions indicate the 68% and 95% confidence limits, respectively. *Left*: The hyperparameters were optimized for the reconstruction. *Right*: Marginalization over the hyperparameters using MCMC methods.

B. Optimization using different covariance functions

Figure 4 shows example reconstructions of $w(z)$ for all models and covariance functions. The different covariance functions have been applied to the same realisation of the data for each model. While the reconstructions using different covariance functions show similar features for a given realisation, we can also see some differences. For our examples, these differences are most obvious for the “peak” model. The squared exponential clearly fails to reconstruct the model, whereas the Matérn functions capture it within the 95% CL.

V. COVERAGE TESTS

When applying GP to a large variety of problems, the true function is *on average* captured within the $1\text{-}\sigma$ ($2\text{-}\sigma$) limits for 68% (95%) of the input range. However, when applying GP to a specific problem (in our case the reconstruction of dark energy), it is not guaranteed that we obtain the same amount of coverage. For a specific problem – and in our case any given EOS – this coverage depends on the choice of covariance function.

For each model, we created 500 mock data sets and performed reconstructions of $w(z)$ for all data sets and covariance functions. Averaging over all realisations for each model, we then determined the fraction of input

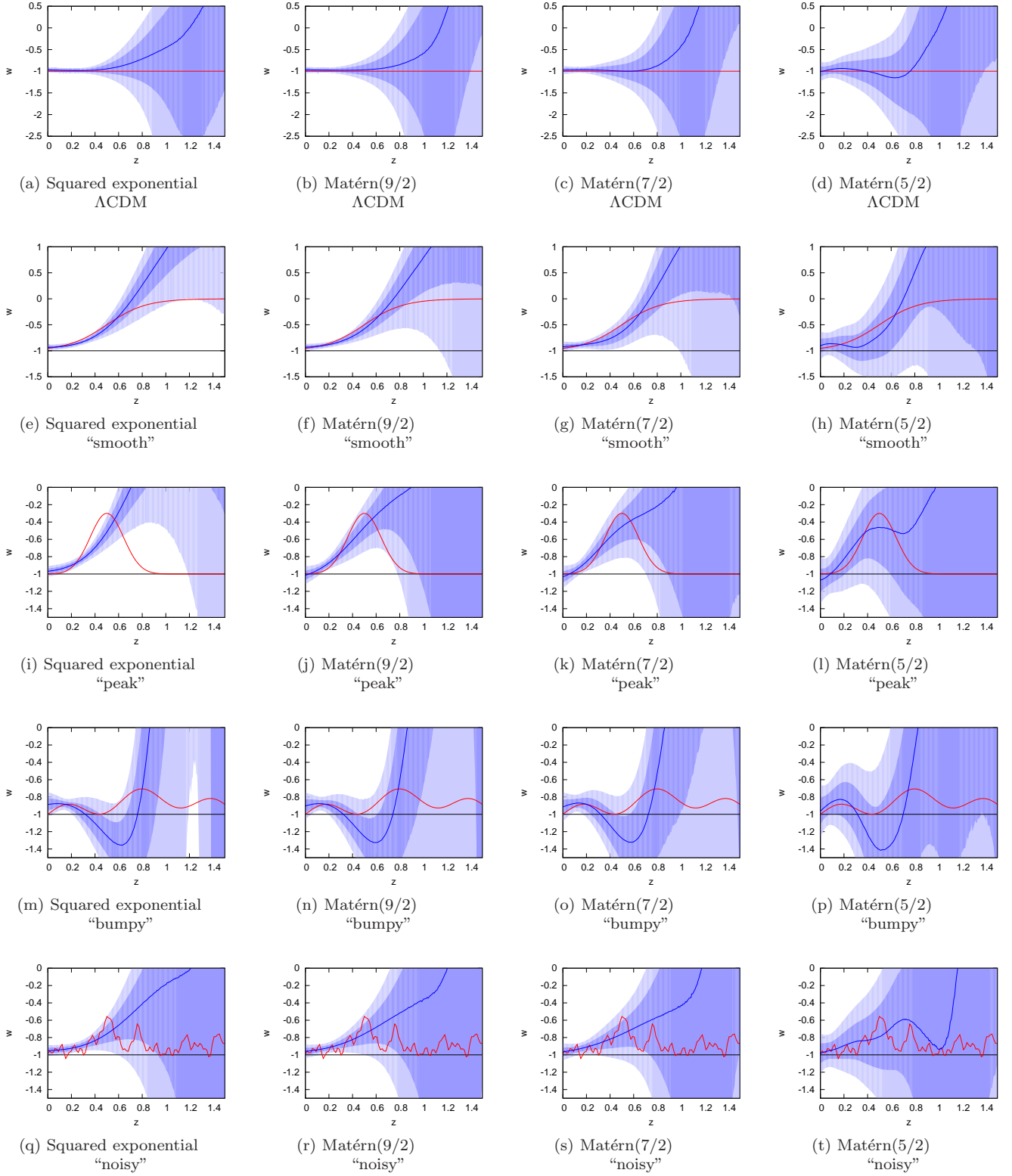


FIG. 4. Gaussian process reconstructions of $w(z)$ from a mock data set for different cosmological models and using different covariance functions. The blue line is the mean of the reconstruction and the blue shaded regions indicate the 68% and 95% confidence limits, respectively. The input model is given by the red line.

function points lying between the reconstructed 1- and 2- σ limits, respectively, for each covariance function and each redshift point. The result is shown in figure 5.

Table II lists these fractions averaged over redshift and also shows the results for the reconstructions of D , D' , D'' and q . The covariance functions are listed in the order of decreasing peak width, i.e. decreasing ν . Recall that the squared exponential corresponds to Matérn(∞). GP are a distribution over functions, which consists of functions of different smoothness. Covariance functions with wider peak lead to a stronger preference of smooth functions in this distribution due to the stronger correlation of function points for $|z - \tilde{z}| \lesssim 2\ell$ (see figure 1). Scales larger than 2ℓ are not relevant for our purposes as the considered redshift range is much smaller than 2ℓ (using the optimized value of ℓ) in all cases.

The preference of smooth functions in the GP distribution subsequently leads to smaller error bars for the reconstruction. Thus, for a given input model, we expect lower coverage for covariance functions with wider peaks due to the smaller error bars of the reconstruction. This effect can indeed be seen in the results of table II.

For Λ CDM and the “smooth” model, Matérn(9/2) leads to the most realistic error bars in the sense that the coverage obtained by the simulation is very close to the theoretically expected values of 68% and 95% for the 1- and 2- σ limits, respectively. When using the squared exponential, we obtain a smaller coverage, indicating that the errors are underestimated. In contrast, the errors are overestimated for Matérn(7/2) and Matérn(5/2).

For the models with stronger redshift dependence (“peak”, “bumpy” and “noisy”), Matérn(9/2) and Matérn(7/2) come closest to the theoretically expected values, with Matérn(9/2) underestimating and Matérn(7/2) overestimating the error bars.

VI. CONSISTENCY WITH A MODEL

GP provide a method for non-parametric reconstructions directly from observational data. But often one would like to know whether a specific model is consistent with the GP reconstruction. In this section, we will describe how deviations of a model from the GP reconstructions can be quantified. We explain the method by means of an example, namely Λ CDM. The technique can be applied to other models analogously. For the reconstructions, we use the Matérn(9/2) covariance function, which was shown in section V to provide the most reliable results for our purposes.

We create 1000 mock Λ CDM data sets, using the scatter and redshift distributions as described in section III. For each data set, we reconstruct w and determine the fraction of the redshift range, in which the fiducial Λ CDM model is captured by the 1-, 2- and 3- σ limits, corresponding to 68.3%, 95.4% and 99.7% CL, respectively of the reconstruction. Note that here we determine this fraction for each realisation of the data individually,

which is in contrast to the averaging over all mock data sets that has been done in Section V.

Figure 6 summarizes the obtained fractions as histograms. For roughly one third of the mock data sets, the fiducial model is captured within the 1- σ limits of the reconstruction over the complete redshift range. For 983 out of 1000 data sets, it is captured within the 3- σ limits over the whole redshift range. While we expect the fiducial model to lie within the 1- σ limits *on average* over 68% of the redshift range, the histogram shows a very large spread of the actual percentages for the individual realisations of the data. For a given data set, it is not unusual to find that the fiducial model is captured within the 1- σ limits anywhere between 10% and 100% of the redshift range. When we consider the 2- σ limits, small percentages become less likely. For the 3- σ limits, we can expect a coverage close to 100%.

We can use these histograms to quantify deviations of the reconstructions from Λ CDM when applying GP to a data set, which may or may not represent Λ CDM. As the 1- σ limits allow for a large range of percentages and thus offer very little constraints, the 2- and 3- σ limits are more suitable for this test. For example, if we find that Λ CDM is captured within the 3- σ limits of the reconstruction over 95% of the redshift range, we can exclude this model at a 99.6% CL as we only found smaller coverage values for 4 out of 1000 mock data sets. Or if Λ CDM is captured within the 2- σ limits over only 50% of the redshift range, then Λ CDM can be ruled out at a 98.3% CL.

In order to quantify deviations for a different model, we would need to produce histograms using mock data sets which assume exactly that model. Also note that when applying the method to a real world problem, it is necessary to create mock data sets using the scatter and redshifts of the actual data set.

VII. CONCLUSIONS

We analyzed various aspects of using GP to reconstruct dark energy from distance measurements. The main questions addressed in this paper were how to choose a suitable covariance function and how to quantify deviations of a model from the GP reconstruction. The presented methods can be applied to other problems analogously.

In theory, the fiducial model that was used to create a mock data set should be captured within the 1- σ (2- σ) limits of the GP reconstruction for 68% (95%) of the input range. These are average values when GP are applied to a variety of different problems. These values do not necessarily apply if we use GP for a specific problem — in our case the reconstruction of dark energy from SN data. We tested various covariance functions on mock data sets for different cosmological models to determine which function recovers the theoretical coverage values for the reconstruction of w .

While Matérn(7/2) provides very good results for the

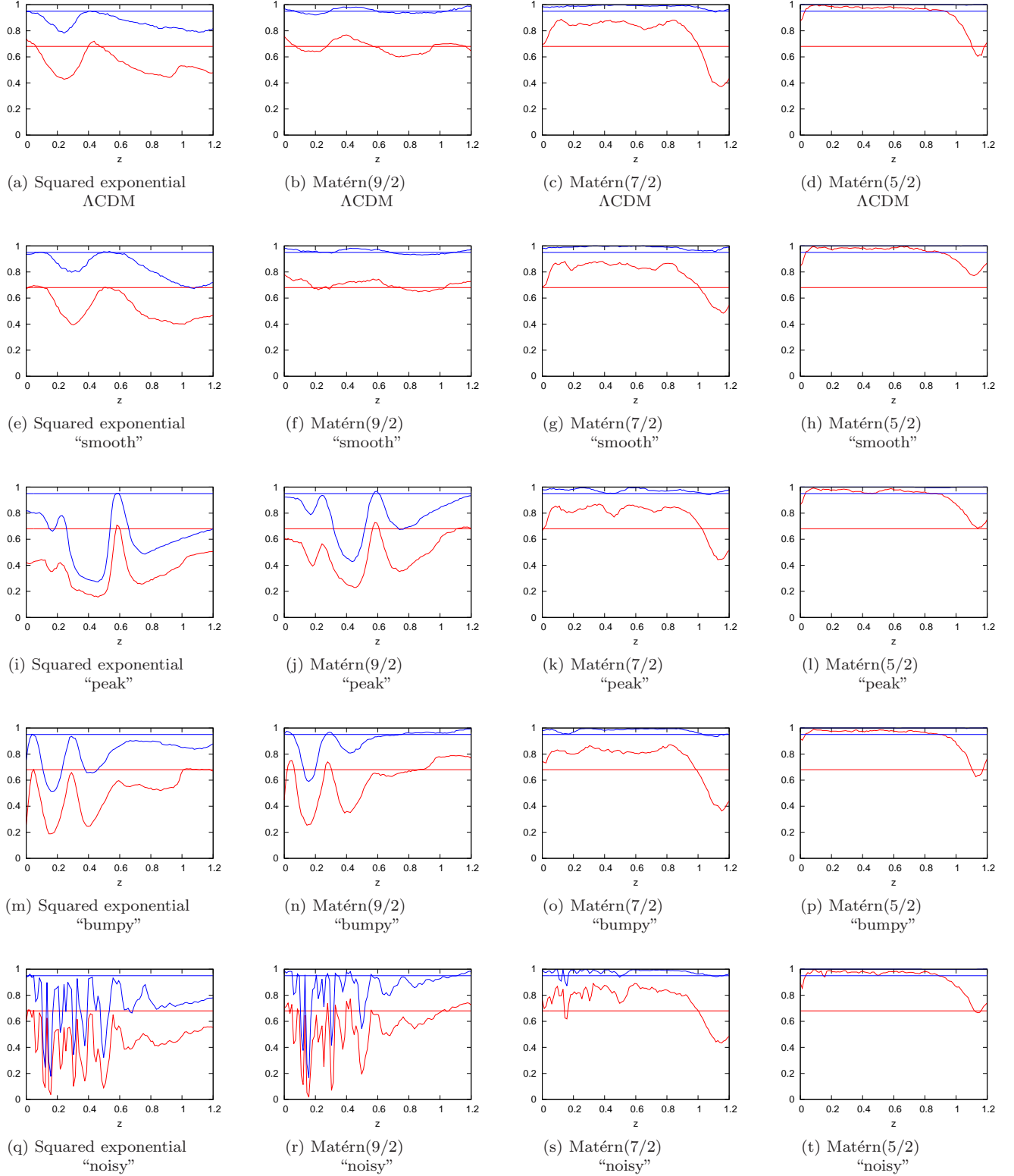


FIG. 5. Coverage test for $w(z)$ using 500 mock data sets for different cosmological models and using different covariance functions. Shown is the fraction of input model points captured with the $1\text{-}\sigma$ (red) and $2\text{-}\sigma$ (blue) limits of the reconstructions. The constant red and blue lines indicate the theoretically expected values 0.68 and 0.95, respectively.

	Squared exp.	Matérn(9/2)	Matérn(7/2)	Matérn(5/2)	Squared exp.	Matérn(9/2)	Matérn(7/2)	Matérn(5/2)
ACDM								
D	0.636	0.676	0.685	0.728	0.924	0.950	0.952	0.968
D'	0.580	0.661	0.712	0.793	0.899	0.947	0.963	0.985
D''	0.518	0.684	0.770	0.934	0.851	0.960	0.989	1.000
w	0.542	0.676	0.776	0.929	0.863	0.953	0.985	1.000
q	0.521	0.678	0.774	0.937	0.850	0.954	0.987	1.000
Smooth								
D	0.663	0.703	0.696	0.723	0.935	0.955	0.952	0.966
D'	0.595	0.695	0.727	0.794	0.904	0.953	0.966	0.985
D''	0.505	0.707	0.784	0.940	0.823	0.963	0.988	1.000
w	0.524	0.702	0.785	0.945	0.836	0.956	0.987	1.000
q	0.516	0.702	0.787	0.945	0.833	0.957	0.987	1.000
Peak								
D	0.544	0.604	0.691	0.724	0.868	0.912	0.950	0.965
D'	0.437	0.539	0.720	0.788	0.739	0.850	0.961	0.980
D''	0.337	0.480	0.770	0.927	0.568	0.773	0.973	1.000
w	0.361	0.491	0.774	0.926	0.598	0.781	0.973	0.999
q	0.344	0.482	0.775	0.932	0.575	0.770	0.973	0.999
Bumpy								
D	0.621	0.663	0.679	0.717	0.925	0.931	0.950	0.968
D'	0.569	0.638	0.707	0.783	0.890	0.929	0.961	0.983
D''	0.479	0.605	0.751	0.931	0.793	0.902	0.981	1.000
w	0.506	0.605	0.756	0.929	0.812	0.906	0.978	1.000
q	0.482	0.601	0.755	0.936	0.795	0.899	0.979	1.000
Noisy								
D	0.621	0.671	0.693	0.718	0.927	0.953	0.956	0.964
D'	0.565	0.649	0.720	0.793	0.875	0.941	0.964	0.981
D''	0.406	0.544	0.752	0.934	0.698	0.853	0.977	1.000
w	0.440	0.559	0.760	0.929	0.733	0.865	0.975	0.999
q	0.414	0.547	0.757	0.937	0.704	0.852	0.975	1.000

TABLE II. Coverage test of the Gaussian process for different models and covariance functions. *Left*: Fraction of function points lying between the $1\text{-}\sigma$ limits. In each line, the fraction closest to the theoretical value 0.68 has been highlighted. *Right*: Fraction of function points lying between the $2\text{-}\sigma$ limits. In each line, the fraction closest to the theoretical value 0.95 has been highlighted.

reconstruction of D for all models, it overestimates the errors for the reconstructions of the derivatives of D . If one is only interested in D itself, but not in its derivatives or any derived quantities, then Matérn(7/2) is the best choice.

We found that the Matérn(9/2) covariance function leads to excellent results for Λ CDM and the “smooth” model for all reconstructed quantities, but tends to underestimate the errors for the other models. This is caused by the fact that GP in general prefer the reconstructed functions to be smooth if there is no sufficient evidence for rapid variations. The strength of this preference depends on the choice of covariance function: the wider the peak of the covariance function, the stronger the preference for a smooth reconstruction.

We recommend the Matérn(9/2) covariance function

for the reconstruction of dark energy with current supernovae data as it provides reliable results for the smoothest reconstructions that are consistent with the data. However, keep in mind that it does not pick up rapid variations in w if there is insufficient evidence for these variations. In such a case, the errors will be underestimated, and for a more conservative estimate one should use a smaller ν .

In general these results are indicative of a general trend for the reconstruction of w , but for substantially increased numbers of SNIa, very different errors or distributions, and different considerations in the families of EOS one might be interested in, this analysis should be extended. Once the numbers of SNIa becomes sufficiently large, more complicated covariance functions with different length scale parameters could also be considered for

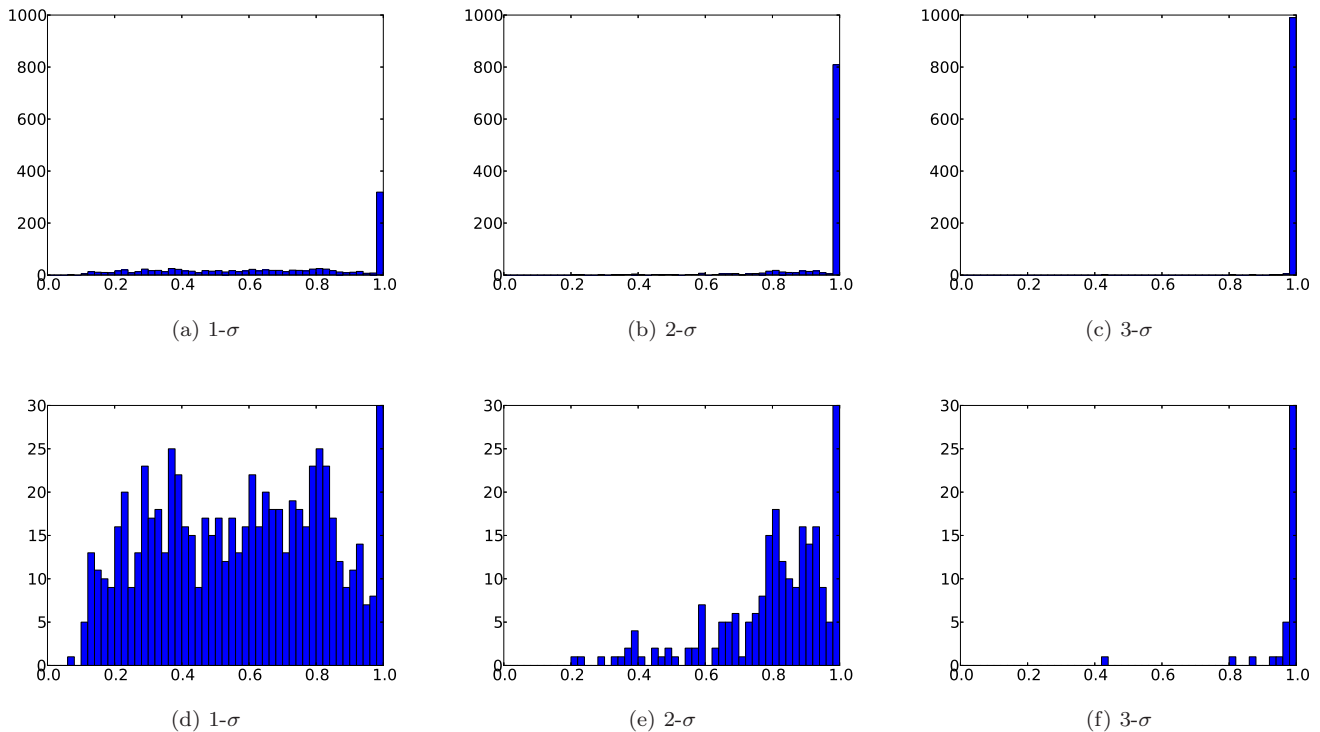


FIG. 6. Histograms of the percentages of the redshift range, where the fiducial Λ CDM model is captured by the 1-, 2- and 3- σ limits of the reconstructions of w for a given realisation of the data. In total, 1000 mock data sets have been used. The bottom row shows a zoomed-in version of the plots in the top row.

complicated EOS.

We introduced a way to quantify deviations of a model from the GP reconstructions. The coverage obtained for the actual data set needs to be compared to the distribution of coverages of many mock data sets. The input model for the mock data sets needs to be identical to the model one wishes to test. The number of mock data sets with a larger coverage than the one for the observed data

determines the CL at which the model can be rejected.

ACKNOWLEDGMENTS

MS was supported by the South Africa Square Kilometre Array Project and the South African National Research Foundation (NRF). CC was supported by the NRF.

-
- [1] E. J. Copeland, M. Sami, and S. Tsujikawa, *Int.J.Mod.Phys.* **D15**, 1753 (2006), arXiv:hep-th/0603057 [hep-th].
- [2] T. Clifton, P. G. Ferreira, A. Padilla, and C. Skordis, *Phys.Rept.* **513**, 1 (2012), arXiv:1106.2476 [astro-ph.CO].
- [3] C. Clarkson, B. Bassett, and T. H.-C. Lu, *Phys.Rev.Lett.* **101**, 011301 (2008), arXiv:0712.3457 [astro-ph].
- [4] C. Zunckel and C. Clarkson, *Phys.Rev.Lett.* **101**, 181301 (2008), arXiv:0807.4304 [astro-ph].
- [5] V. Sahni, A. Shafieloo, and A. A. Starobinsky, *Phys.Rev.* **D78**, 103502 (2008), arXiv:0807.3548 [astro-ph].
- [6] A. Shafieloo and C. Clarkson, *Phys.Rev.* **D81**, 083537 (2010), arXiv:0911.4858 [astro-ph.CO].
- [7] S. Nesseris and A. Shafieloo, *Mon.Not.Roy.Astron.Soc.* **408**, 1879 (2010), arXiv:1004.0960 [astro-ph.CO].
- [8] M. Seikel, S. Yahya, R. Maartens, and C. Clarkson, *Phys.Rev.* **D86**, 083001 (2012), arXiv:1205.3431 [astro-ph.CO].
- [9] M. Seikel, C. Clarkson, and M. Smith, *JCAP* **1206**, 036 (2012), arXiv:1204.2832 [astro-ph.CO].
- [10] S. Yahya, M. Seikel, C. Clarkson, R. Maartens, and M. Smith, (2013), arXiv:1308.4099 [astro-ph.CO].
- [11] T. Holsclaw, U. Alam, B. Sanso, H. Lee, K. Heitmann, *et al.*, *Phys.Rev.* **D82**, 103502 (2010), arXiv:1009.5443 [astro-ph.CO].

- [12] T. Holsclaw, U. Alam, B. Sanso, H. Lee, K. Heitmann, *et al.*, Phys.Rev.Lett. **105**, 241302 (2010), arXiv:1011.3079 [astro-ph.CO].
- [13] T. Holsclaw, U. Alam, B. Sanso, H. Lee, K. Heitmann, *et al.*, Phys.Rev. **D84**, 083501 (2011), arXiv:1104.2041 [astro-ph.CO].
- [14] A. Shafieloo, A. G. Kim, and E. V. Linder, Phys.Rev. **D85**, 123530 (2012), arXiv:1204.2272 [astro-ph.CO].
- [15] A. Shafieloo, A. G. Kim, and E. V. Linder, Phys.Rev. **D87**, 023520 (2013), arXiv:1211.6128 [astro-ph.CO].
- [16] R. Nair, S. Jhingan, and D. Jain, (2013), arXiv:1306.0606 [astro-ph.CO].
- [17] M. Kunz, Phys.Rev. **D80**, 123001 (2009), arXiv:astro-ph/0702615 [astro-ph].
- [18] C. Clarkson, M. Cortes, and B. A. Bassett, JCAP **0708**, 011 (2007), arXiv:astro-ph/0702670 [astro-ph].
- [19] R. Hlozek, M. Cortes, C. Clarkson, and B. Bassett, General Relativity and Gravitation **40**, 285 (2008), arXiv:0801.3847 [astro-ph].
- [20] C. E. Rasmussen and C. K. I. Williams, *Gaussian Processes for Machine Learning* (The MIT Press, 2005).
- [21] D. Foreman-Mackey, D. W. Hogg, D. Lang, and J. Goodman, PASP **125**, 306 (2013), arXiv:1202.3665 [astro-ph.IM].
- [22] J. Bernstein, R. Kessler, S. Kuhlmann, R. Biswas, E. Kovacs, *et al.*, Astrophys.J. **753**, 152 (2012), arXiv:1111.1969 [astro-ph.CO].